Hindawi
Advances in Civil Engineering
Volume 2020, Article ID 8812277, 15 pages
https://doi.org/10.1155/2020/8812277

Research Article

Stability Analysis of a Two-Layered Slope with Cracks by Finite Element Limit Analysis

Ai-zhao Zhou,[1] **Gang Liu**,[1] **Xian-wen Huang**,[1,2] **Peng-ming Jiang**,[1] **and Yu Chen**[3]

[1]*School of Architecture and Civil Engineering, Jiangsu University of Science and Technology, Mengxi Road, Zhenjiang, Jiangsu, China*
[2]*School of Civil Engineering and Architecture, Anhui University of Science and Technology, Huainan, Anhui, China*
[3]*School of Civil Engineering and Transportation, Hohai University, Xikang Road, Nanjing, Jiangsu, China*

Correspondence should be addressed to Xian-wen Huang; 994310735@qq.com

Received 23 September 2020; Revised 13 October 2020; Accepted 3 November 2020; Published 20 November 2020

Academic Editor: Yong Liu

In this study, to support slope stability estimating engineering, the stability of a slope with cracks lying on two-layered slopes was investigated by a self-developed adaptive element limit analysis (AFELA) code. Upper bound (UB) and lower bound (LB) results of soil additional gravity factor SF within 4% relative error were obtained to quantify the effects of several factors, including the Moore–Cullen strength ratio, angle of the slope, thickness of the top layer, length of the crack, angle of the crack, and crack's distance from the edge. Typical failure patterns were also discussed for deeper insight into the two-layered slope stability with cracks. In addition, the results of the AFELA code were compared with the actual situation of the slope and existing commercial calculation software to verify the reliability of this investigation.

1. Introduction

The in situ geological survey report shows that, due to the influence of dry–wet cycles [1], erosion caused by rainfall [2], and human disturbances, there may be a large number of initial cracks in the shallow slope, and the existence of these cracks will affect the stability of the slope [3, 4]. When a slope with cracks is in a rainy environment, rainwater will invade the depths of the slope along the cracks. The increase in soil water content will not only reduce the shear strength of the soil, but also increase the gravity. Both will reduce the stability of the slope [5–7]. When a slope with cracks is subjected to dynamic loads such as earthquakes [8], the existence of initial cracks will greatly weaken the stability of the slope, causing local landslides [9] or overall landslides, endangering people's lives and property [10]. Based on a field investigation and model test, Zhang et al. [9] proved that the initial crack distribution is a potential problem causing slope instability; Krzeminska et al. [11] pointed out that the distribution of cracks in the slope is related to the hydrological environment, which will affect the stability of the slope. In addition, according to the research results of He et al. [12], cracks often appear on the slope surface and at the top of the slope. The appearance of cracks at the top of the slope has the greatest impact on the stability of the slope, because it may directly affect the failure mode [13]. Therefore, it is necessary to study the stability of a slope with cracks on the top.

In order to evaluate slope stability, designers have proposed many methods, such as the semiempirical formula method [9], limit equilibrium method [14–17], slip line method [6, 18], and upper and lower limit solutions [19, 20], but these methods first assume a specific slip line. However, when relying on some parameters and engineering experience to determine the sliding type (arc, logarithmic spiral [21], etc.) and location of the slip line [22, 23], this does not guarantee the reliability of the slope stability analysis. With the development of slope calculation theory and the advancement of computer technology, the method of numerical analysis has gradually been promoted, which has overcome the problem of preassuming slope failure surface. Cheng et al. [23] compared the calculation results of limit analysis and strength reduction method [24] in slope stability and proved the reliability of limit analysis in calculating the stability of homogeneous soil slopes. Liu et al. [25]

used the finite element method to study the stability of the soil–rock slope and obtained the real slope plastic development zone; Zhou et al. [26] used limit analysis to study the influence of uneven distribution of soil strength on slope stability. In recent years, the limit stability analysis method with adaptive function has often been used for slope stability analysis. This method can efficiently and reliably calculate the slope stability [20, 27, 28].

In the existing slope stability analysis process with cracks, the slope material is generally simplified as homogeneous. However, in a real slope, due to geological structure, sedimentation, and other factors, the soil is settling. The process has obvious layering characteristics [29–31]. The research results of Favre et al. [11, 32–34] showed that the failure mode of double-layer soil slopes is significantly different from that of single-layer soil slopes, but there are few related studies in this area [29]. The analysis results of Li et al. [35] also reached the same conclusion. When a two-layer slope includes cracks, the depth and position of the cracks will affect the stability of the slope [36, 37]. Through model tests and numerical analysis, Huang et al. [25] proved that the distribution of cracks will have an impact on slope stability. After that, Utili et al. [38] conducted in-depth research on the stability of cracked slopes, but their research conclusions are not sufficient to guide engineering applications.

Based on the previously mentioned analysis and research conducted on a slope support project in Zhenjiang City, Jiangsu Province, this paper uses improved adaptive limit analysis software to study the stability of a double-layered soil slope with cracks. The specific research contents are as follows: (1) multifactor parameter research is carried out, and the change trend of the slope safety factor is explained in the design chart, (2) revealing the influence of these influencing factors on the slope failure mode and summarizing several typical slope failure modes, and (3) the calculation results of the adaptive limit analysis software are compared with the analysis results of the engineering site and Optum G2, which verifies the reliability of the numerical model.

2. Problem Definition

Figure 1 shows a real slope support project in Zhenjiang City, Jiangsu Province. Under the effect of rainfall, cracks with varying degrees of influence appeared on the top of the slope. Dislocation, tension cracks, and slight landslides occurred in the soil layer, which affected the stability of the slope. If the slope has a landslide, it could cause damage to the industrial plant at the foot of the slope, so it is necessary to conduct a stability assessment of the slope. Through the on-site geological survey, it can be found that the slope is a typical double-layer soil slope with initial cracks on the top of the slope. Affected by the geological structure and human activities, there are certain differences in the Moore–Cullen strength ratio, the angle of the slope, thickness of the top layer, length of the crack, angle of the crack, and crack's distance from the edge. Therefore, in order to better evaluate the slope stability, it is necessary to understand the influence of these factors on the slope stability and failure mode.

According to the geological survey report, the geometric dimensions of a typical slope surface are as follows. As shown in Figure 1, the slope height is 10 m, the slope angle β is 45°, the distance D between the crack and the slope is 2 m, the length of the shallow crack L is 1.5 m, and the top layer thickness T is 5 m. It should be noted that the conclusion of geological survey report is based on the on-situ investigation, geological conditions, surrounding engineering cases, and survey results from geological radar, comprehensively. According to the Geotechnical Test Regulations, the measured strength parameters (cohesion and internal friction angle) of the top and bottom soils are 8 kPa and 18° and 10.67 kPa and 23.42°, respectively. In order to fully consider the influence of crack distribution on slope stability, combined with the results of a crack soil strength test, the crack strength parameters are considered as 0.1 kPa and 0.1°, respectively.

In order to objectively analyze the influence of various influencing factors on slope stability (the Moore–Cullen strength ratio of the angle of the slope, thickness of the top layer, length of the crack, angle of the crack, and crack's distance from the edge), a dimensionless slope stability analysis model is determined. The standard dimensionless top layer strength of the Moore-Cullen model (*S*.MC) is set to 1.0 (8 kPa, 18°), and the corresponding calculation equation is shown in (1) [24, 25]. The adjusted range of *S*.MC is set to 0.5–1.5; the slope angle β is set to 30°–60°; the crack angle α is set to 60°–120°; the dimensionless distance between crack and slope D/H is set to 0–0.25; the dimensionless length of crack L/H is set to 0.05–0.3; and the dimensionless thickness of top layer T/H is set to 0.1–0.6. It should be noted that some ranges of the previously mentioned research variables are low possibility of occurrence in practice, but it is meaningful and typical for better presenting the failure modes of slope with cracks.

$$\text{S.MC} = \frac{c_s}{c_a} = \frac{\tan \varphi_s}{\tan \varphi_a}. \tag{1}$$

Combined with the influencing factors of a double-layered slope with cracks, the safety factor of slope can be described as follows:

$$\text{SF} = f\left(\text{S.MC}, \alpha, \beta, \frac{D}{H}, \frac{L}{H}, \frac{T}{H}\right). \tag{2}$$

3. Analytical Method

3.1. AFELA Model. In recent years, due to higher calculation accuracy and efficiency, finite element limit analysis (FELA) has been widely used in slope stability analysis. Compared with the previous slope limit analysis method, FELA solves the problem that the slope sliding belt needs to be assumed in advance (circular arc, spiral, etc.), which makes the calculated slope slip surface closer to the real slope failure surface. In the calculation process, by separately solving the slope velocity field and stress field, the strict upper limit solution [39] and lower limit solution [40] of the slope stability can be obtained. Based on the obtained upper limit solution and lower limit solution, the real slope stability value and the corresponding slope shear surface can be obtained. In order to obtain accurate calculation results of

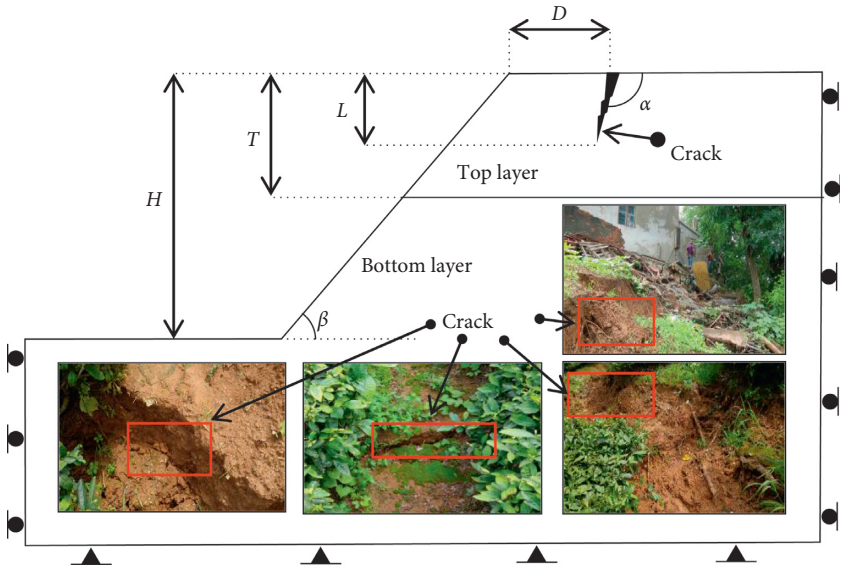

Figure 1: Definition of two-layered slope with cracks.

slope safety factor, the discontinuous finite element calculation equations of the upper limit solution and lower limit solution are introduced [41, 42]. The use of discontinuous finite element formulation in the static form of limit analysis leads to two nonlinear optimization models that can be presented in the same form:

$$\text{Minimize: } \lambda, \tag{3}$$

$$\text{Subject to: } B^T\sigma = g_0 + \lambda g, \tag{4}$$

$$f\left(\sigma_j\right) \le 0, \quad j = 1, \ldots, n_\sigma, \tag{5}$$

where λ is the load multiplier of additional gravity; is the operator of discrete equilibrium type, $\sigma = (\sigma_1, \ldots, \sigma_{n\sigma})^T$ is the vector of σ_j; n_σ is the sum of discrete stresses, g_0 and g are the vectors of gravity and prescribed gravity; and f is the yield function.

In order to solve equations (3)–(5), the authors proposed a nonlinear optimization algorithm, which is an optimization of the arc interior point algorithm [43, 44]. In order to ensure the accuracy and efficiency of the calculation, an adaptive meshing method based on the energy method is proposed. The calculation process of this method mainly includes the following:

(1) The input of the initial grid parameters, including the number of basic elements (B.E.), number of remeshing elements (M.E.), and number of repeat times (R.T.).

(2) As shown in Figure 2(a), mesh the slope and perform the first limit analysis.

(3) Search for the remeshing area and the corresponding remeshing elements based on the strain, stress, or shear dissipated energy.

(4) Grid remeshing, as shown in Figure 2(b): the higher the strain, stress, and shear dissipated energy is, the greater the density of the mesh is; after remeshing is finished, the slope stability is analyzed again.

(5) Repeat steps 3 and 4 until the designed remeshing times are reached. Figures 2(c)–2(e) show the slope meshing results when the number of repeats is three, four, and five, respectively; it can be seen from Figure 3 that as the densification increases, the mesh density of the slope shear zone area becomes larger and the calculation result is more accurate.

In order to determine the appropriate meshing parameters, different initial meshing elements and remeshing elements and times are set, and the slope safety factor calculation results are as shown in Figure 3. Among them, the slope safety factor is the average value of the upper limit solution and the lower limit solution of the slope gravity increase coefficient, as shown in

$$\text{SF} = \frac{\lambda_{\text{UP}} + \lambda_{\text{LP}}}{2}. \tag{6}$$

It can be seen from Figure 3 that as the number of repeats increases, the safety factor and the difference between the upper limit solution and the lower limit solution are gradually reduced, and greater reducing amplitude appeared when the repeat times number three or fewer. Hence, it can be concluded that three is the most suitable number of repeats. In addition, by comparing the results with different meshing elements, it can be observed that, with the increase in the number of basic meshing elements, the safety factor accuracy is higher, and 8000 is recognized as the highest number of suitable basic elements that leads to both great accuracy and calculation efficiency.

3.2. Model Rationality Verification. The research results of Huang et al. [9, 16, 45] showed that the slope will have certain precursors before a landslide, such as crack at slope, soil dislocation, and vegetation tilt. At this time, the safety factor of the slope should be 0.98–1.02. When the slope safety factor is higher than 1.02, the slope should be in a

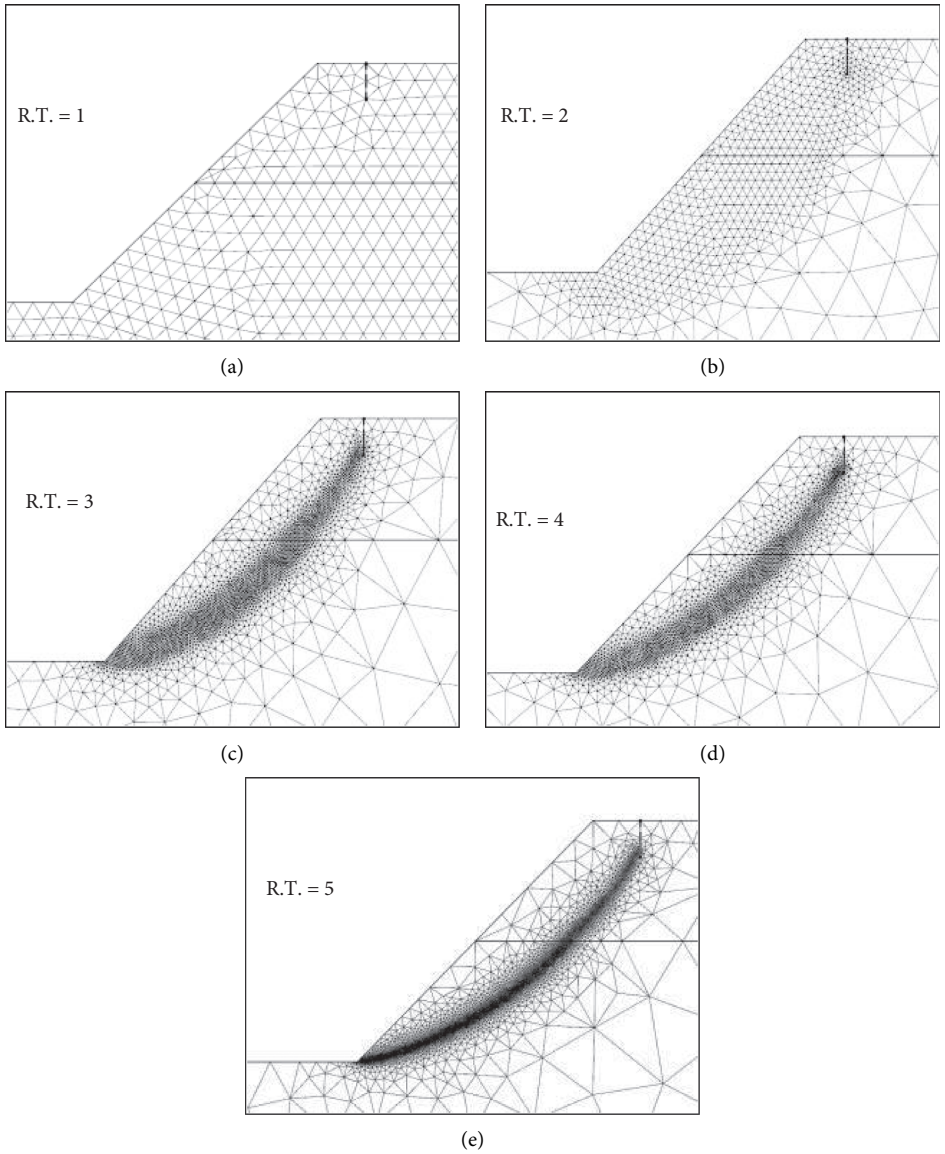

Figure 2: Meshing results of slope. (a) R.T. = 1. (b) R.T. = 2. (c) R.T. = 3. (d) R.T. = 4. (e) R.T. = 5.

stable state, which is different from a condition where the slope is about to slide. When the slope safety factor is lower than 0.98, the slope should have already produced a landslide, which contradicts the on-site situation, where the slope has not yet slipped. The calculation result of slope stability in this paper is 1.005, which is in the range of 0.98–1.02. Therefore, the analysis result of this model can be considered reasonable.

Optum G2 is a widely accepted commercial finite element limit analysis calculation software, and the rationality of its calculation results has been verified by Wu et al. [20]. Therefore, this software is used to verify the reliability of the calculation results in this paper. It can be seen from Figure 4 that, with the increase in the dimensionless strength S. MC of the top layer, the slope safety factor continues to increase. The analytical results of this paper and Optum G2 have the same trend in the calculation results. Comparing the relative error of the slope safety factor calculation of the two (7), it can be seen that the difference between the two is always small and the relative error calculated by AFELA is smaller than those calculated by OptumG2, so the method proposed in this paper is reasonable. In terms of stability of calculation results, comparing the calculation results of Optum G2 and the algorithm in this paper, it can be seen that the upper and lower safety factors of the slope using the algorithm in this paper are included in the upper and lower limits of Optum G2, and the difference between the upper and lower limits is more stable than with Optum G2. This shows that the grid encryption algorithm in this paper has certain computational advantages over Optum G2, mainly in terms of computational accuracy and stability.

$$\text{Error} = \left| \frac{2(A - B)}{A + B} \right| \cdot 100\%. \tag{7}$$

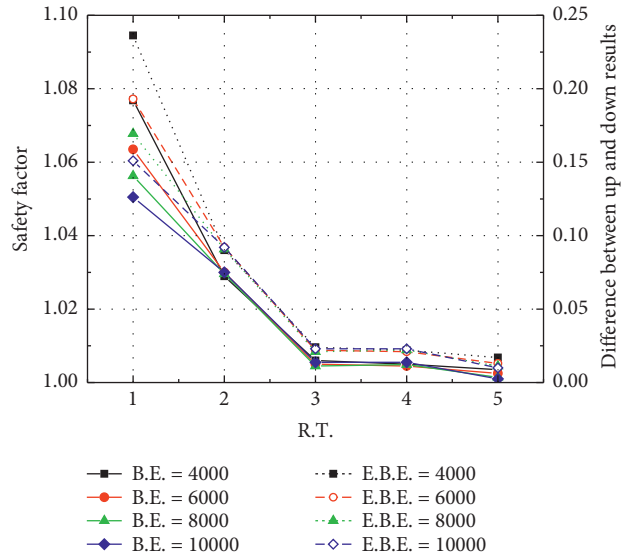

Figure 3: Slope stability under different initial grid elements and remeshing times.

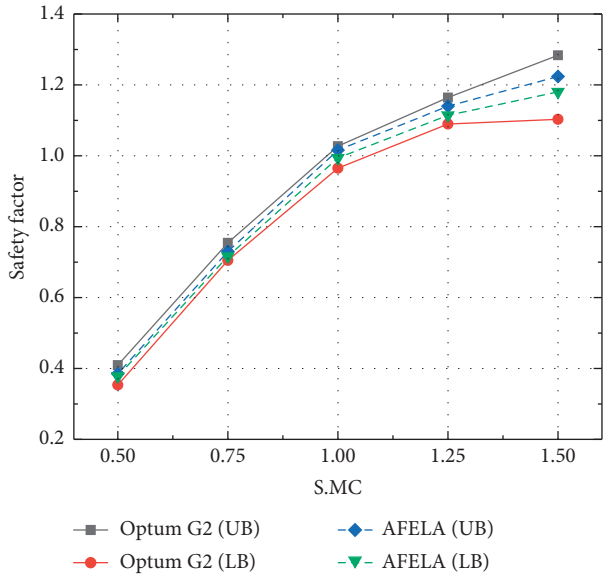

Figure 4: Comparison of calculation results of slope safety factor.

4. Results and Discussion

This chapter analyzes in detail the influence of each variable in equation (2) on the stability of a two-layered slope with cracks and summarizes the corresponding failure mode of the slope under the influence of each variable.

4.1. Effect of Dimensionless Strength of Top Layer. It can be seen from Figure 5 that, with the increase in S. MC, the safety factor of the slope increased gradually in total, but with a different change tendency under different variables. For the standard group ($\alpha = 90^{\circ}$, $\beta = 45^{\circ}$, $D/H = 0.2$, $L/H = 0.15$, $T/H = 0.5$), when the S. MC is smaller than 1.0, with the increase in S. MC, the safety factor shows greater increasing amplitude; when the S. MC is larger than 1.0, the safety factor shows lower increasing amplitude. Comparing the safety factor of the standard group, the $D/H = 0.1$ (the crack close to the slope), and the $L/H = 0.05$ group (the crack length is small), it can be observed that the difference between the three is small with different S. MC values. Hence, it can be concluded that the distance between the crack and the slope and the crack length were less affected by the S. MC. Comparing the results between the standard group and $\alpha = 120^{\circ}$ group, it can be seen that the changing tendency of the safety factor with S. MC is similar, but the $\alpha = 120^{\circ}$ group is smaller than the standard group under the given S. MC. When the T/H (the top layer thickness is small) is set to 0.3, the S. MC is smaller than 1.25 and the safety factor of the $T/H = 0.3$ group is greater than the standard, but when the S. MC is larger than 1.25, the opposite tendency appears. Furthermore, it should be observed that the safety factor of the T/H = 0.3 group is always greater than 1.0. When the slope angle β is set to 30°, the safety factor of the slope increased rapidly with the increase of S. MC. Only when the S. MC is 0.5 is the safety factor of the slope lower than 1.0; otherwise, the safety factor of the slope is always greater than 1.0.

Based on the previously mentioned analysis with different S. MC, it can be concluded that (1) the distance between crack and slope D/H and the crack length L/H have a little effect on the slope safety; (2) the greater crack angle α will lead to a lower safety factor; (3) the reduction of top layer thickness T/H and slope angle β will increase the safety factor of the slope. In addition, by analyzing the failure modes of two-layer slope with cracks at different S. MC, it can be concluded that the slope tends to partial failure mode at a low S. MC (shown in Figure 6(a)) and the failure surface is from the toe of the top layer to the bottom of the crack; as shown in Figure 6(b), the slope tends toward overall failure, and the failure surface is from the toe of slope to the bottom of the crack. The different failure mode can be explained by the antisliding force caused in the top layer [35, 45]. When the strength of top layer is lower which means lower antisliding force, the shear surface will develop from the toe of top layer to the crack and form partial failure. When the strength of top layer is higher, the shear surface will develop from the toe of slope to the bottom of crack and form overall landslide.

Figure 7 shows the four typical shear failure surfaces of a two-layer slope with cracks at S. MC = 1.5, including (1) a partial landslide without through cracks; (2) a deep landslide without through cracks; (3) an overall landslide with through cracks; and (4) an overall landslide without through cracks. As shown in Figure 7(a), S. MC = 1.5 and $\beta = 30^{\circ}$, and the slope shows a partial landslide without through cracks. This can be explained by the smaller slope angle β. As shown in Figure 7(b), when the S. MC is large (S. MC = 1.5) and the distance between slope and crack is small (D/H = 0.1), the slope shows an overall landslide without through cracks. This can be explained by the high strength of the soil making the shear surface deeper and the crack being close to the slope, which leads to an overall landslide without through cracks. As shown in Figure 7(c), when the S. MC is great (S. MC = 1.5), the development of the shear surface is exactly through the cracks, and the failure surface consists of the shear surface and crack. As shown in Figure 7(d), when the crack angle is large ($\alpha = 120^{\circ}$), the shear surface developed from the toe of the

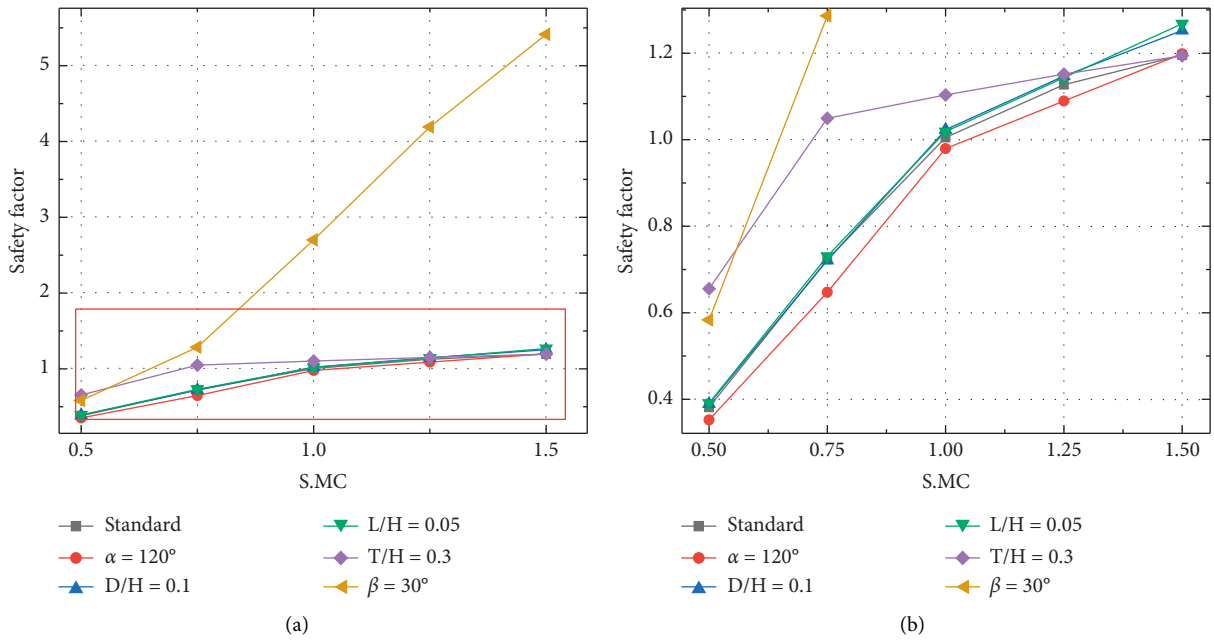

Figure 5: The influence of top layer strength on slope stability. (a) Calculation results. (b) Partial calculation results.

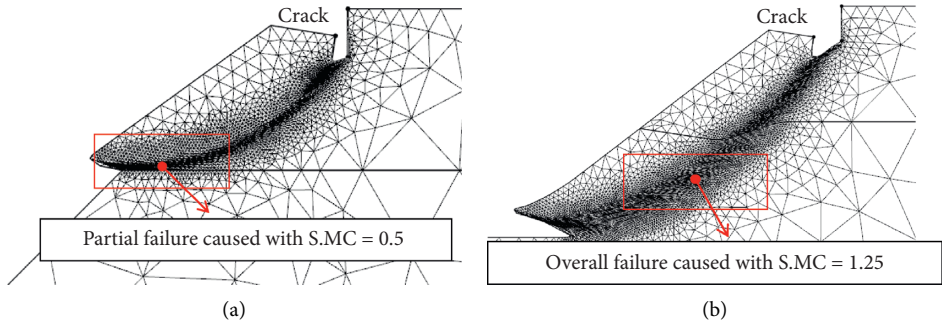

Figure 6: The failure modes of slope at different S. MC values. (a) S. MC = 0.5. (b) S. MC = 1.25.

slope to the bottom of the crack. As shown in Figure 7(e), when the thickness of top layer is low (T/H = 0.3) and the S. MC is high (S. MC = 1.5), the shear surface develops from the toe of slope to the bottom of crack and forms an overall landslide through the crack. As shown in Figure 7(f), when the S. MC is high (S. MC = 1.5) and the crack length is small (L/H = 0.05), the failure surface will bypass the crack and form a deep landslide without through cracks, which is related to the minor weakening effect of the crack on slope stability.

Based on the analysis of the slope stability and failure surface at different S. MC, it can be concluded that the influence of the top layer on slope stability mainly involves two aspects. On the one hand, under low strength, the slope is prone to partial landslides instead of the traditional overall landslide. On the other hand, a change in the top layer strength will affect the shear surface developing path.

4.2. Effect of Slope Angle. Figure 8 shows the slope safety factor under different slope angles. It can be seen from the figure that as the slope angle increases, the slope safety factor continues to decrease, and the amplitude gradually decreases. For the standard group, the safety factors at the slope angles of 30°, 45°, and 60° are 2.779, 1.005, and 0.610, respectively, and the reduction amplitudes are 1.774 and 0.395, respectively. When the slope angle β was set to 30°, it was found that (1) when crack angle α was 120°, the slope safety was is smaller than the standard group; (2) when the crack was close to the slope (D/H = 0.1) or the crack length was large (L/H = 0.3), the slope safety factor was similar to the standard; (3) when the top layer strength was high (S. MC = 1.5) or the thickness of top layer was small (T/H = 0.3), the slope safety was higher than the standard. In addition, it can also be observed that (4) all the slope safety factors are larger than 1.0, which means that the slope is stable.

In premise of slope angle $\beta = 45°$, when the crack angle is larger ($\alpha = 120°$), the crack is close to the slope (D/H = 0.1), the crack length is long (L/H = 0.3), the top layer strength is high (S. MC = 1.5), or the thickness of the top layer is small (T/H = 0.3), the safety factor of the slope is always larger than the standard group and 1.0. When the slope angle β is 60°, the safety factor of slope with different affecting character is similar to the standard group and smaller than 1.0. It means that the Moore–Cullen strength ratio, the angle of the slope,

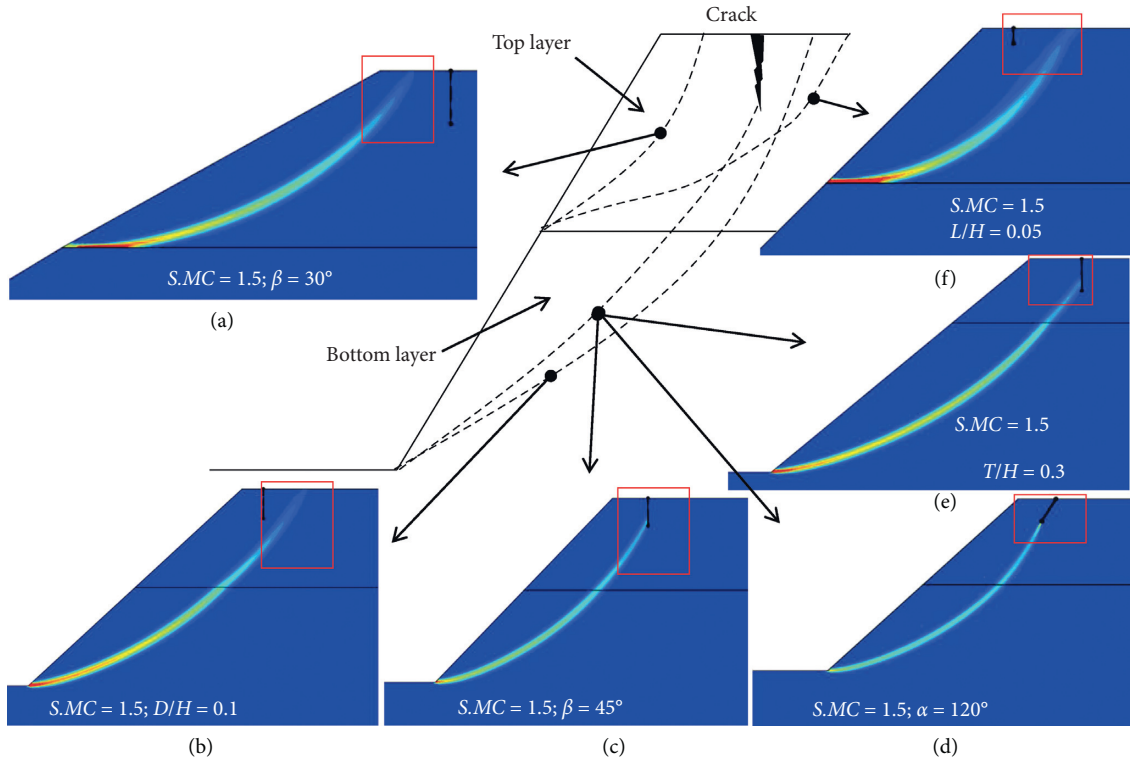

Figure 7: Typical failure modes of two-layer slope with cracks.

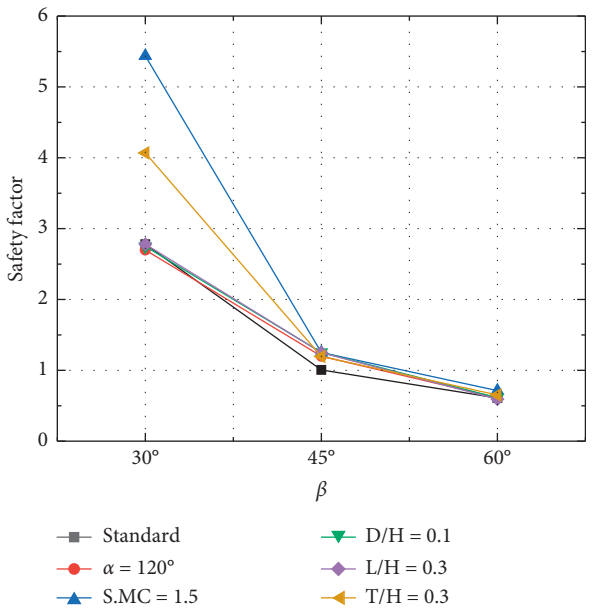

Figure 8: The influence of slope angle on slope stability.

thickness of the top layer, length of the crack, angle of the crack, and crack's distance from the edge have less influence on the slope safety factor when the slope angle β is 60°.

Figure 9 shows the failure surface of a two-layer slope with cracks at different slope angles. For better presenting the shear failure zones, referring to Gao's studies [20], the deformation of elements was enlarged 3~100 times. It can be seen from Figure 9(a) that when the slope angle was 30°, partial failure occurred and the failure surface only consisted of the shear surface that developed from the toe of the top layer to the slope top. At this point, the slope had the maximum safety factor, which was larger than 1.0. As shown in Figure 9(b), when the slope angle was 45°, the slope showed overall landslide and the failure surface consisted of the shear surface and crack. When the slope angle was 60°, as shown in Figure 9(c), the failure surface was similar to that in Figure 9(b), but some difference appeared at the top of the slope, which tends to lead to secondary partial failure.

Figure 10 shows four typical failure modes of a two-layer slope with cracks at 30 degree crack angles. As shown in Figure 10(a), the failure surface developed from the toe of the top layer to the top of the slope and only consisted of a shear surface without through cracks. This can be explained for the less slope angle β. As shown in Figures 10(b) and 10(c), the slope shows an overall failure and the failure surface developed from the toe of the slope to the top of the slope without including the crack. This can be explained by the low thickness of the top layer and the high strength of the top layer, respectively. The lower the thickness of the top layer is and the higher the strength of top layer is, the shallower the shear surface is. Hence, the failure surface developed from the toe of the slope to the top of the slope without contacting the crack. As shown in Figure 10(d), the failure surface developed from the toe of slope to the bottom of crack and formed a partial landslide. It can be explained by the greater crack angle that inducing the development of shear surface. As shown in Figure 10(e), the failure surface developed from the toe of top layer to the middle of crack and formed a partial failure consisting of shear surface and part of crack. It can be explained by the small distance between slope and crack.

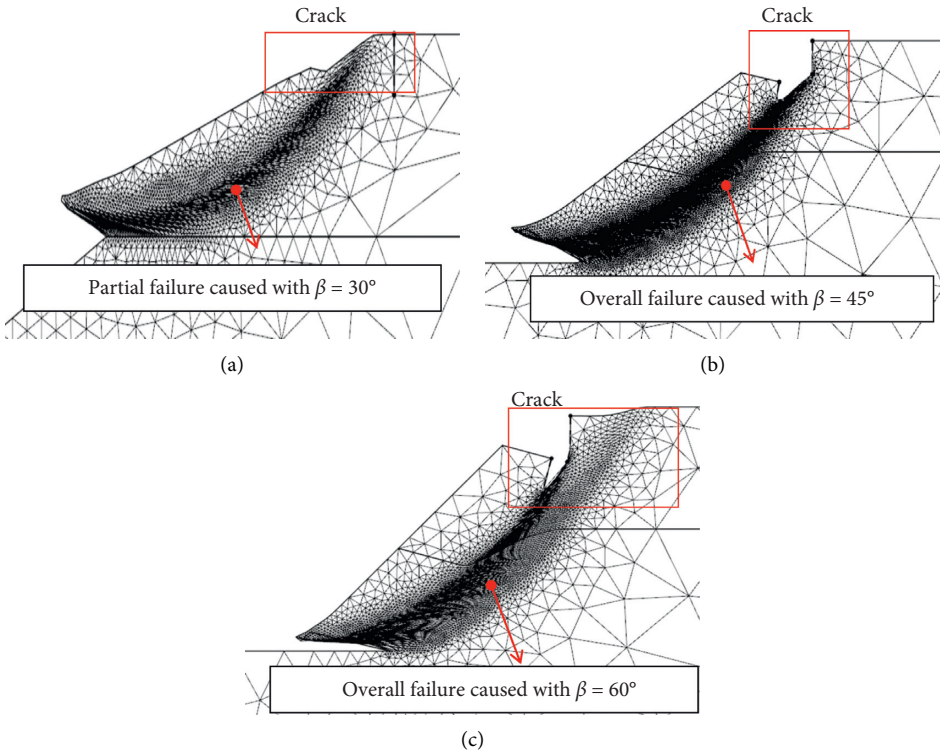

Figure 9: The failure surface of slope at different slope angles. (a) $\beta = 30^{\circ}$. (b) $\beta = 45^{\circ}$. (c) $\beta = 60^{\circ}$.

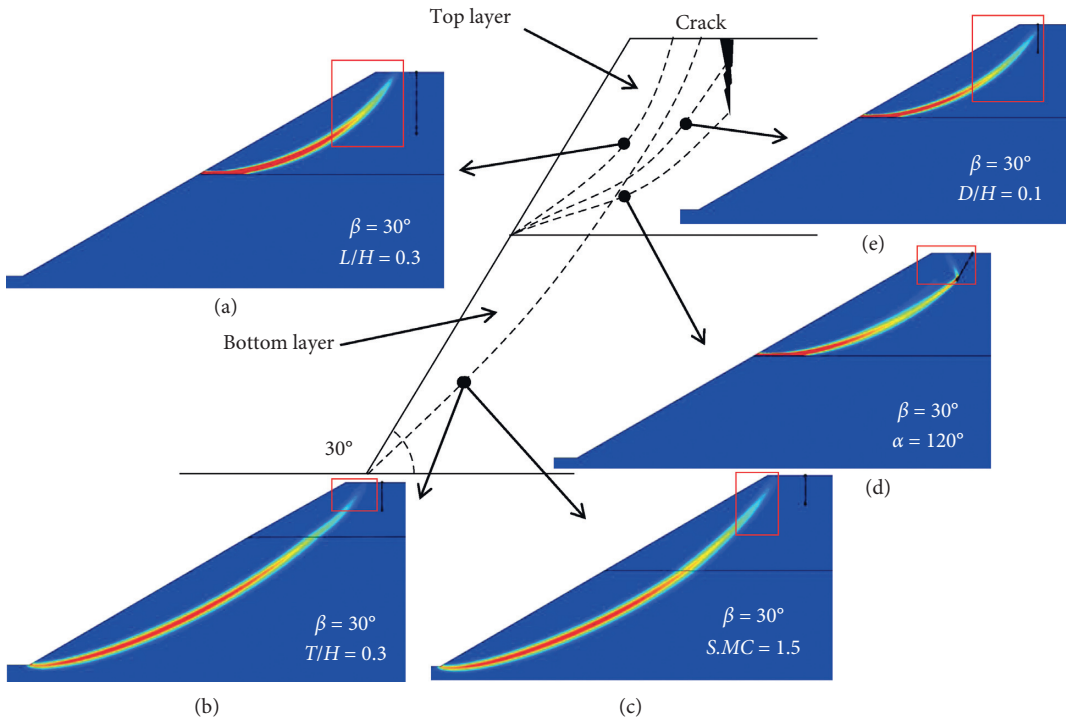

Figure 10: Typical failure modes at different crack angles.

Combining the slope safety factor and failure mode, we find that the effect of slope angle on the safety factor and failure mode of the slope is great. When the slope angle is small, it tends to appear as a shallow landslide without through cracks, and the slope obtains a greater safety factor. When the slope angle is large, it tends to appear as a deep landslide and obtains a lower safety factor.

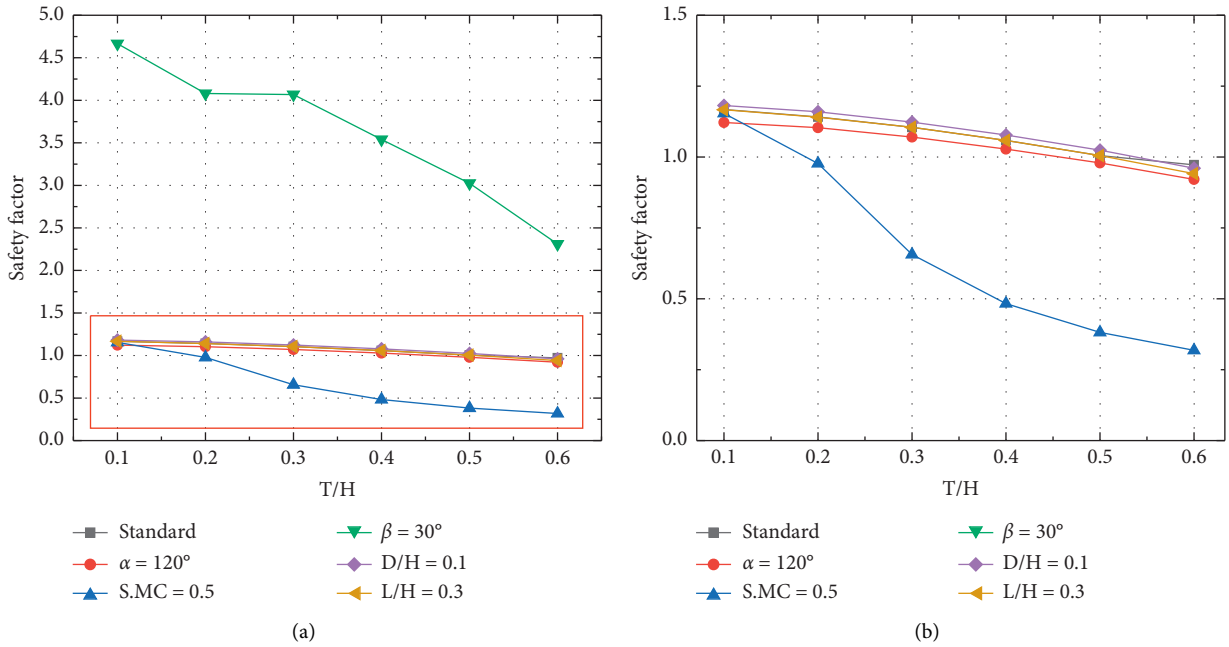

Figure 11: The influence of the thickness of the top layer on slope stability. (a) Calculation results. (b) Partial calculation results.

4.3. Effect of Top Layer Thickness. Figure 11 shows the influence of the thickness of the top layer on slope stability. It can be concluded that, with the increase in top layer thickness, the safety factor of the slope reduced gradually, but the reducing amplitude was different. Comparing the safety factors of the standard group and the $\alpha = 120^{\circ}$ group, we observe that the safety factor of the $\alpha = 120^{\circ}$ group was always smaller than the standard at the same T/H. When the strength of the top layer was low (S. MC = 0.5), with the increase in T/H, the safety factor of the slope rapidly decreased. When the slope angle was small ($\beta = 30^{\circ}$), the safety factor of slope was always larger than 1.0. When the crack was close to the slope, compared to the safety factor of the slope, the safety factor of the $D/H = 0.1$ group was larger than that of the standard group. When the length of crack L/H increased to 0.3 and T/H was smaller than 0.5, both safety factors were similar, but when T/H was larger than 0.5, the slope with the longer crack had a lower safety factor than the standard.

As shown in Figure 12, the failure surface of the slope consisted of the shear surface and crack, but the length of the shear surface in the top layer was different. As shown in Figure 12(a), the thickness of the top layer was small, and less shear surface distributed in the top layer. As shown in Figure 12(b), when the thickness of the top layer was large, there was a greater shear surface lying on the top layer. Because the top layer was low in strength, with more shear surface, there was lower antisliding force to the sliding body, which means a lower safety factor. Hence, it can be concluded that the influence of the top layer's thickness on the slope is mainly manifested in the antisliding force.

Based on the previously mentioned analysis of the slope safety factor under different topsoil depths and the corresponding shear surface development model, it can be concluded that as the thickness of the upper soil increases, the slope safety factor gradually decreases. The main reason is the lower strength of the topsoil, so the failure surface provides less sliding resistance. Among all the influencing factors, when the topsoil strength is low and the thickness is large, the slope will produce a local landslide phenomenon of the topsoil; when the topsoil thickness is thin, the slope tends to produce a whole landslide. In the geological survey process, when the strength of the upper soil is low, special attention should be paid to the influence of the thickness of the topsoil on the slope stability.

4.4. Effect of the Distance between Crack and Slope. Figure 13 shows that, with the increase in distance between the crack and the slope, the safety factor of the slope changes little. For the standard group, the change in amplitude is 0.01 and the safety factor of the slope is always greater than 1.0. When the crack angle was 120°, the changing amplitude of the safety factor was smaller, within 0–0.15 D/H, which is larger than 1.0; when D/H was larger than 0.15, great reducing amplitude appeared and the safety factor was smaller than 1.0. When the S. MC was set to 0.5, the safety factor of the slope was always smaller than 0.5, and the changing amplitude under different D/H was 0.01. When the slope angle was small ($\beta = 30^{\circ}$), the changing amplitude of safety factor under different D/H was 0.05 and always higher than 1.0. When the crack length was greater (L/H = 0.3), the safety factor of the slope was similar to the standard. When the T/H was set to 0.3, the changing amplitude of the safety factor was 0.02 and always greater than that of the standard group. Hence, it can be concluded that (1) a reduction in the slope angle and top layer thickness will improve the slope safety factor; (2) a reduction in the top layer strength will reduce

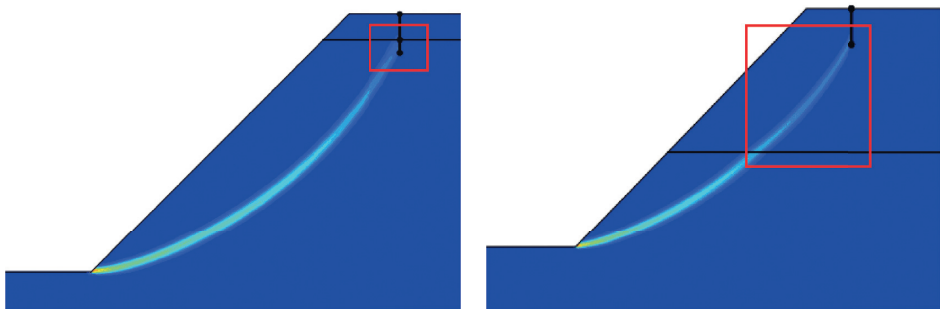

(a) (b)

Figure 12: Failure surface at different thicknesses of top layer. (a) $T/H = 0.1$. (b) $T/H = 0.6$.

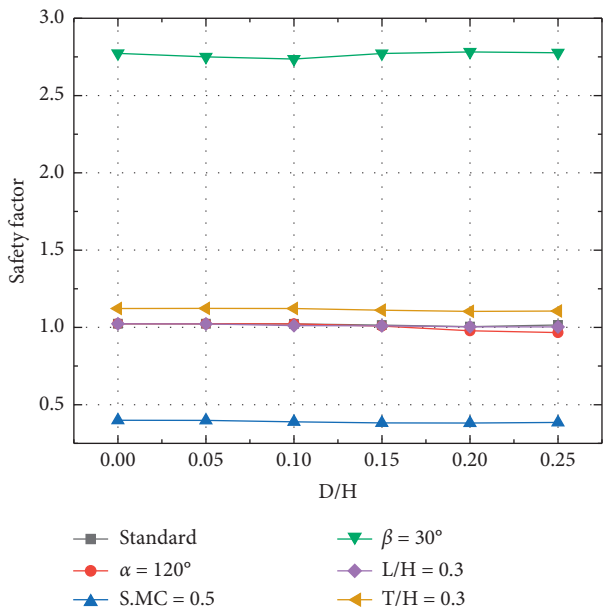

Figure 13: The influence of the distance between crack and slope on slope stability.

the slope safety; (3) the crack length have less effect on the slope stability with different D/H; (4) when the distance between the slope and the crack is greater, a greater crack angle will lead to a low safety factor.

As shown in Figure 14, when the crack position changes, according to the relative position of the shear surface and crack, three typical failure modes will be obtained: (1) including failure, as shown in Figure 14(a), the crack is close to the slope, and the development of the failure surface is not affected by the crack; (2) combining failure, as shown in Figure 14(b), the presence of a crack will affect the development direction and length of the shear surface; the failure surface consists of the shear surface and part of the crack; (3) away failure, as shown in Figure 14(c), the crack is away from the shear surface and has less effect on the slope failure surface.

4.5. Effect of Crack Length. Figure 15 shows the influence of the crack length on slope stability. For the standard group, with the increase in crack length, the safety factor of slope gradually decreased, but the reducing amplitude was small (0.016). When the crack angle was 120°, with the increase in crack length L/H, the safety factor of the slope gradually decreased, and a greater reducing amplitude appeared when the crack length L/H was larger than 0.15. The total reducing amplitude of the slope was 0.136. When the top layer strength S. MC was 0.5, the safety factor of the slope was smaller than 0.5, and the total reducing amplitude was 0.012. When the slope angle was small, the safety factor of the slope was far larger than 1.0, and the corresponding reducing amplitude was 0.005. When the distance between the crack and the slope was small, the safety factor of the slope was similar to that of the standard group. When the thickness of the top layer was small, the safety of the slope was larger than 1.0 and surpassed that of the standard group.

Figure 16 shows the different failure modes of a two-layer slope with cracks at different crack depths. As shown in Figure 16(a), the crack length was small. The shear surface developed from the toe of the slope to the crack nearby. When the length of the crack increased, as shown in Figure 16(b), the shear surface developed from the toe of slope to the bottom of the crack, and the failure surface consisted of the shear surface and crack. When the length of crack L/H reached 0.3, the shear surface developed from the toe of slope to the middle of the crack (shown in Figure 16(c)), and the failure consisted of the shear surface and part of the crack. This can explain the smaller induced effect of the crack on the development of the slope shear surface [25]. When the crack was large (120°), the induced effect of the crack on the development of the slope shear surface improved, and the shear surface developed toward the bottom of crack, as shown in Figures 16(d) and 16(e). In addition, comparing the length of the shear surface in Figures 16(d) and 16(e), it can be observed that the shear surface length in Figure 16(d) is larger, which means that more antisliding force appeared in the sliding body. Hence, the slope stability in Figure 16(d) is larger than that in Figure 16(e).

Based on the previously mentioned analysis and discussion of slope safety factors and the development path of the shear surfaces, it can be concluded that when the slope angle of the crack is 120°, the change in the depth of the crack has a greater impact on the safety factor of the slope. The main reason is related to the full play of the "induction

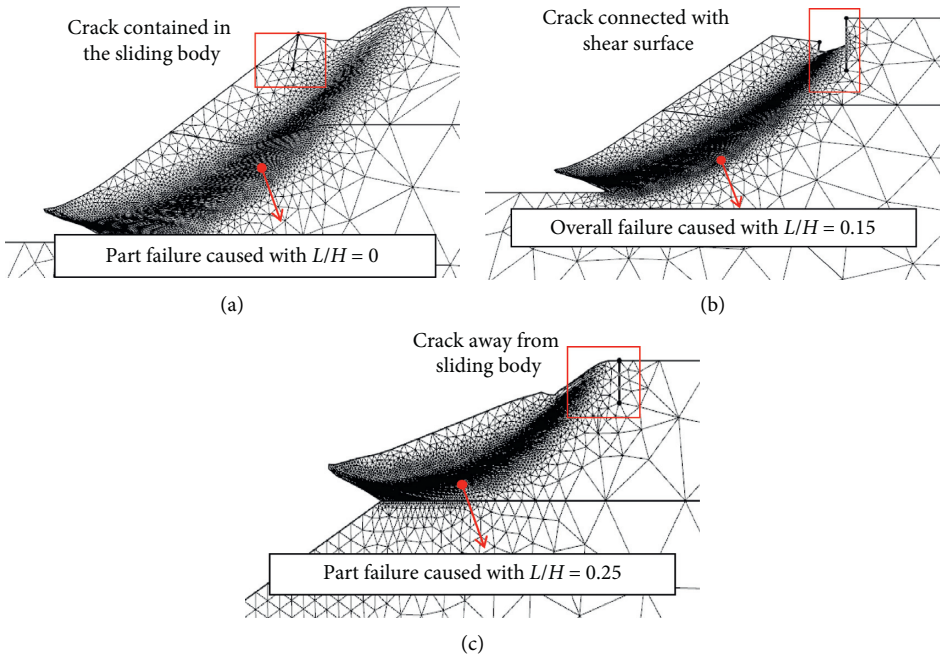

Figure 14: Failure modes of slope under different distances between crack and slope. (a) D/H = 0. (b) D/H = 0.15. (c) D/H = 0.25.

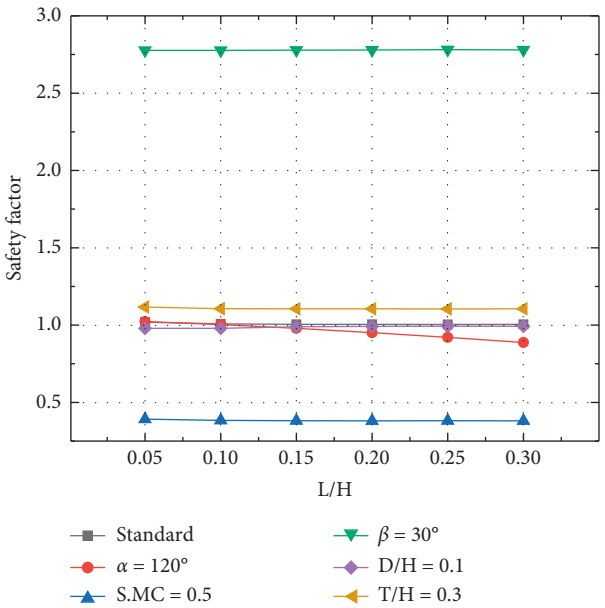

Figure 15: The influence of the crack length on slope stability.

effect" of the crack on 1ptthe shear surface. "Induction effect" means that the failure surface tends to develop in the direction of weak zones in the slope, and it is detailed in Liu's studies [25]. The other factors are less sensitive to the change in slope crack length. When the slope forms a combined failure surface of shear surface and crack, the longer the length of the crack, the shorter the length of the shear surface, the smaller the antisliding force produced by the sliding body, and the lower the safety factor of the slope.

4.6. Effect of Crack Angle. As shown in Figure 17, with the increase in crack angle, the safety factor of the slope gradually decreased, but the reducing amplitude was different. For the standard group, the safety factor of the slope decreased slowly, and the reducing amplitude was 0.035. With a long crack length (L/H = 0.3), when the rock angle was smaller than 90°, the safety factor of the slope was less affected by the crack; when the crack angle was larger than 90°, a greater reducing amplitude appeared with the increase in crack angle and the safety factor of the slope was smaller than 1.0. When the top layer was low in strength (S. MC = 0.5), the reducing amplitude of the safety factor of the slope was 0.042, and the safety factor of the slope was smaller than 1.0. When the crack was close to the slope (D/H = 0.1), with the increase in crack angle, the safety factor of the slope slowly decreased, and the reducing amplitude was 0.009. When the slope angle was small ($\beta = 30°$), the safety factor of the slope was larger than 1.0 and the changing amplitude was small (0.007). When the thickness of the top layer was smaller (T/H = 0.3), the safety factor of the slope was larger than the standard, and the changing amplitude was 0.044. The sensitivity relationship of each factor to the safety factor of the slope was crack length > top layer (dimensionless thickness) > soil (dimensionless strength) > standard group > distance between crack and slope > slope angle.

As shown in Figure 18, which compares the development path of the slope surface with crack angles of 60° and 120°, when the crack angle is larger, the overall length of the slope shear surface is smaller than that of the slope with a smaller crack angle, which means the sliding body of the slope provides less antisliding force, and the safety factor of the slope is lower. The failure surface in the two figures is

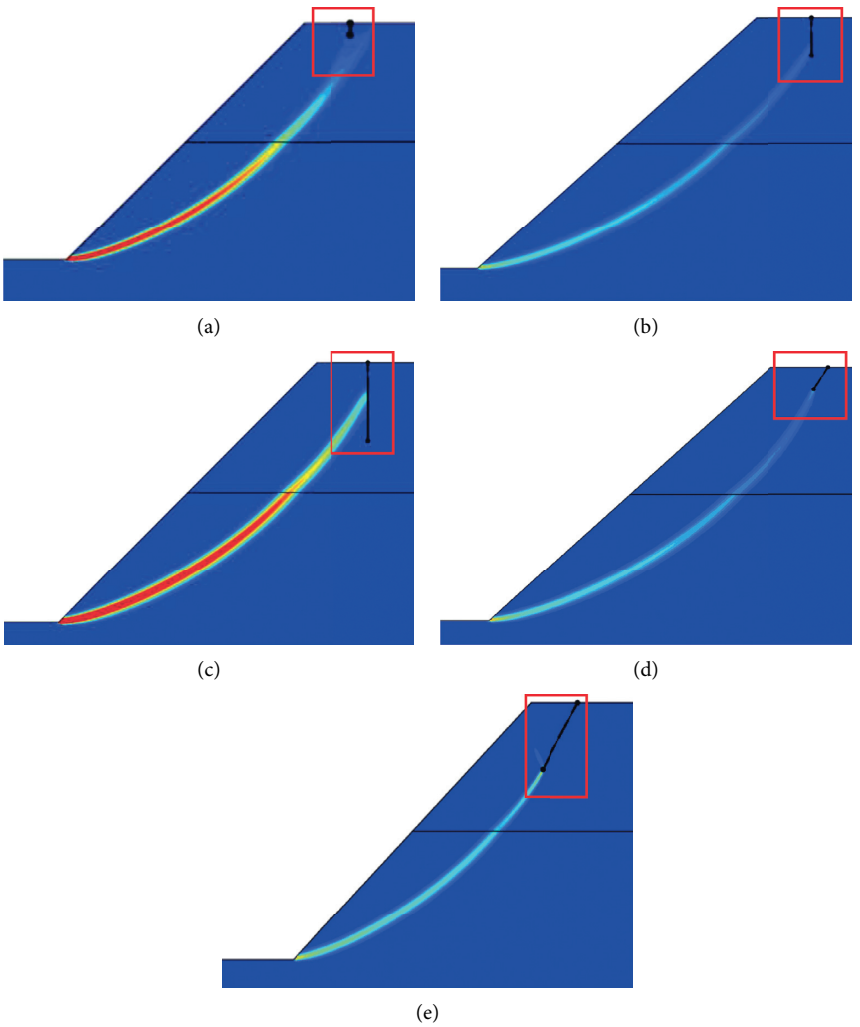

Figure 16: Failure mode of slope at different crack depths. (a) L/H = 0.05. (b) L/H = 0.10. (c) L/H = 0.15. (d) L/H = 0.20. (e) L/H = 0.25.

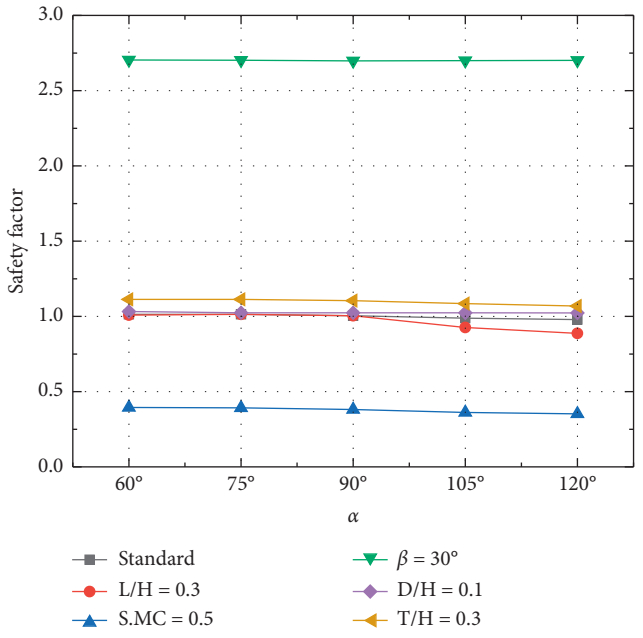

Figure 17: The influence of the crack angle on slope stability.

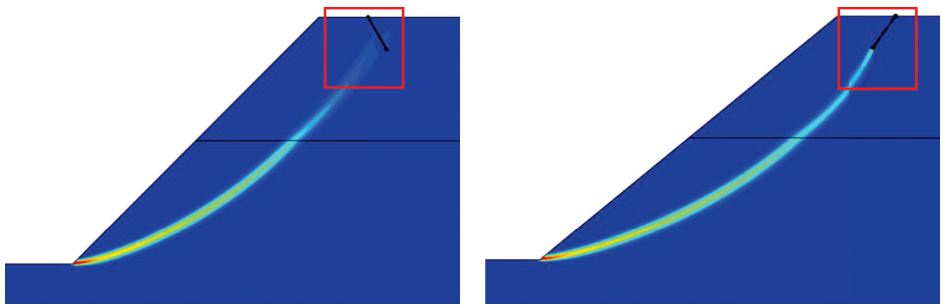

(a) (b)

Figure 18: Failure surface at different crack angles. (a) $\alpha = 60^{\circ}$. (b) $\alpha = 120^{\circ}$.

composed of a combination of shear surface and cracks, but the slope cracks under a large crack angle occupy a larger proportion of the sliding belt, which means that the sliding body provides lower sliding resistance and the safety factor of the slope is small. In addition, the "induction effect" of the crack on the development of the slope shear surface is also the reason for the higher stability of the slope with a small fracture dip. Huang et al. [25] proved that when the development path of the shear surface was parallel to the crack, the safety factor of the slope was lower. Therefore, the safety factor of a slope with a small crack angle is higher than that with a large crack angle.

Synthesizing the slope safety factors under different crack angles and the development path of the shear surface, it can be concluded that when the crack length is large, the change in the crack angle has a greater influence on the slope safety factor. The influence of the safety factor of the slope, with the variation in the inclination of the crack, is mainly manifested in the "induction effect" of the development path of the shear surface and the "shortening effect" of the length of the sliding surface.

5. Conclusions

Based on a slope project in Zhenjiang City, Jiangsu Province, this paper used the self-developed AFELA program to study the stability of a two-layered slope with cracks. Based on the slope section, some potential influencing factors were analyzed. The influence of each influencing factor on the slope safety factor and the development law of the failure surface was analyzed in detail, and the analysis results were compared with the project condition and Optum G2. The specific research conclusions were as follows.

(1) A finite element limit analysis calculation model with self-adaptive function was proposed, and this model was used to study the stability of two-layered slopes with cracks. The results of the model were compared with the calculation results of the project condition and Optum G2 to verify the reliability of the adaptive model.

(2) According to the slope stability analysis under different strengths of top layer, its influence on slope can be summarized as follows: when the top layer strength is low, the slope tends to appear as a partial landslide rather than an overall landslide. The change in top layer strength will affect the developing path of the failure surface; when the top layer strength is high, the failure surface will develop behind the crack and the slope will form a deep landslide without through cracks. In addition, the change in top layer strength will also affect the antisliding force of the sliding body.

(3) Regarding the geometric dimensions of the slope, when the angles of the slope change from small to large, the safety factor of the slope gradually decreases, and the failure mode of the slope changes from partial failure to overall failure; with low top layer strength, when the thickness of the topsoil of the slope changes from shallow to thick, the safety factor of the slope gradually decreases, which is related to the smaller antisliding force on the shear surface passing through the top layer.

(4) In terms of cracks, the safety factor of the slope increases with an increase in the length of the crack, and the effect is most obvious when the crack angle is 120°; the safety factor of the slope generally increases with the increase in the crack angles. In addition, when the crack angle is greater than 90°, the influence of various influencing factors on the slope safety factor is greater than when the crack inclination angle is less than 90°; the slope safety factor generally increases as the distance between the crack and the slope surface increases, but the amplitude is small.

Data Availability

The data used to support the findings of this study are included within the article.

Conflicts of Interest

The authors declare that they have no conflicts of interest.

Acknowledgments

This research was funded by the National Natural Science Foundation of China (grant nos. 51579119 and 41772311) and the Natural Science Fund for Colleges Universities of Jiangsu Province (grant no. 17KJB560003).

References

[1] C.-S. Tang, Y.-J. Cui, B. Shi, A.-M. Tang, and C. Liu, "Desiccation and cracking behaviour of clay layer from slurry state under wetting-drying cycles," *Geoderma*, vol. 166, no. 1, pp. 111–118, 2011.

[2] W. Wang, Y. Li, K. Yao, N. Li, A. Zhou, and C. Zhang, "Strength properties of nano-MgO and cement stabilized coastal silty clay subjected to sulfuric acid attack," *Marine Georesources and Geotechnology*, vol. 38, Article ID 1656313, 2019.

[3] J. Zhang, D. Zhu, and S. Zhang, "Shallow slope stability evolution during rainwater infiltration considering soil cracking state," *Computers and Geotechnics*, vol. 117, Article ID 103285, 2020.

[4] L. Tang, Z. Zhao, Z. Luo, and Y. Sun, "What is the role of tensile cracks in cohesive slopes?" *Journal of Rock Mechanics and Geotechnical Engineering*, vol. 11, no. 2, pp. 314–324, 2019.

[5] C. Sidle and A. Bogaard, "Dynamic earth system and ecological controls of rainfall-initiated landslides," *Earth Science Reviews*, vol. 13, no. 5, pp. 1–23, 2015.

[6] O. Faruk, G. Candan, and E. Murat, "Dynamics of a complex mass movement triggered by heavy rainfall: a case study from NW Turkey," *Geomorphology*, vol. 42, no. 3, pp. 329–341, 2002.

[7] N. Li, S. Lv, W. Wang, J. Guo, P. Jiang, and Y. Liu, "Experimental investigations on the mechanical behavior of iron tailings powder with compound admixture of cement and nano-clay," *Construction and Building Materials*, vol. 254, Article ID 119259, 2020.

[8] Z. Li, X. Yang, and T. Li, "Static and seismic stability assessment of 3D slopes with cracks," *Engineering Geology*, vol. 265, p. 14, Article ID 105450, 2019.

[9] S. Zhang, Q. Xu, and Q. Zahng, "Failure characteristics of gently inclined shallow landslides in Nanjiang, Southwest of China," *Engineering Geology*, vol. 217, pp. 1–11, 2016.

[10] R. P. Chapuis, "Predicting the saturated hydraulic conductivity of soils: a review," *Bulletin of Engineering Geology and the Environment*, vol. 71, no. 3, pp. 401–434, 2012.

[11] D. M. Krzeminska, T. A. Bogaard, T. W. J. van Asch, and L. P. H. vanBeek, "A conceptual model of the hydrological influence of fissures on landslide activity," *Hydrology and Earth System Sciences*, vol. 16, no. 6, pp. 1561–1576, 2012.

[12] Y. He, Y. Liu, Y. Zhang, and R. Yuan, "Stability assessment of three-dimensional slopes with cracks," *Engineering Geology*, vol. 252, pp. 136–144, 2019.

[13] M.-Y. Wang, Y. Liu, Y.-N. Ding, and B.-L. Yi, "Probabilistic stability analyses of multi-stage soil slopes by bivariate random fields and finite element methods," *Computers and Geotechnics*, vol. 122, Article ID 103529, 2020.

[14] J. Bronswijk, "Shrinkage geometry of a heavy clay soil at various stresses," *Soil Science Society of America Journal*, vol. 5, no. 54, pp. 1500–1502, 1990.

[15] V. Chertkov and I. Ravina, "Tortuosity of crack networks in swelling clay soils," *Soil Science Society of America Journal*, vol. 6, no. 63, pp. 1523–1530, 1999.

[16] X. Liu, D. Li, Z. Cao, and Y. Wang, "Adaptive Monte Carlo simulation method for system reliability analysis of slope stability based on limit equilibrium methods," *Engineering Geology*, vol. 264, Article ID 105384, 2019.

[17] K. Qi, Q. Li, and Y. Liu, "Meso-scale investigations on the effective thermal conductivity of multi-phase materials using the finite element method," *International Journal of Heat and Mass Transfer*, vol. 151, Article ID 119383, 2020.

[18] E. Damiano, R. Greco, A. Guida, and L. Olivares, "Investigation on rainwater infiltration into layered shallow covers in pyroclastic soils and its effect on slope stability," *Engineering Geology*, vol. 220, pp. 1–18, 2017.

[19] B. Albrecht and C. Benson, "Effect of desiccation on compacted natural clays," *Journal of Geotechnical and Geoenvironmental Engineering*, vol. 1, no. 127, pp. 67–75, 2001.

[20] G. Wu, R. Zhang, M. Zhao, and S. Zhou, "Undrained stability analysis of eccentrically loaded strip footing lying on layered slope by finite element limit analysis," *Computers and Geotechnics*, vol. 123, Article ID 103600, 2020.

[21] N. Kunitomo and Y. Hakuju, "Bearing capacity analysis of foudations on slopes by use of log-spiral sliding surfaces," *Soils and Foundations*, vol. 3, no. 30, pp. 144–152, 1990.

[22] R. Baker, "Determination of the critical slip surface in slope stability computations," *International Journal for Numerical and Analytical Methods in Geomechanics*, vol. 4, no. 4, pp. 333–359, 1980.

[23] Y. M. Cheng, T. Lansivaara, and W. B. Wei, "Two-dimensional slope stability analysis by limit equilibrium and strength reduction methods," *Computers and Geotechnics*, vol. 34, no. 3, pp. 137–150, 2007.

[24] H. Wang, B. Zhang, G. Mei, and N. Xu, "A statistics-based discrete element modeling method coupled with the strength reduction method for the stability analysis of jointed rock slopes," *Engineering Geology*, vol. 264, Article ID 105247, 2019.

[25] S. Liu, X. Huang, A. Zhou, J. Hu, and W. Wang, "Soil-rock slope stability analysis by considering the nonuniformity of rocks," *Mathematical Problems in Engineering*, vol. 2018, Article ID 3121604, 15 pages, 2018.

[26] A. Zhao, X. Huang, N. Li, P. Jiang, and W. Wang, "A Monte Carlo approach to estimate the stability of soil–rock slopes considering the non-uniformity of materials," *Symmetry*, vol. 12, no. 4, pp. 1–14, 2020.

[27] S. W. Sloan, "Geotechnical stability analysis," *Géotechnique*, vol. 63, no. 7, pp. 531–571, 2013.

[28] D. Griffiths and P. Lane, "Slope stability analysis by ®nite elements," *Geotechnique*, vol. 3, no. 40, pp. 387–403, 1999.

[29] Y. Liu, W. Zhang, L. Zhang, Z. Zhu, J. Hu, and H. Wei, "Probabilistic stability analyses of undrained slopes by 3D random fields and finite element methods," *Geoscience Frontiers*, vol. 9, no. 6, pp. 1657–1664, 2018.

[30] M. Wang, Y. Liu, U. Ding, and B. Yi, "Probabilistic stability analyses of multi-stage soil slopes by bivariate random fields and finite element methods," *Computers and Geotechnics*, vol. 122, p. 103529, 2020.

[31] Y. Liu, Q. He, J. Jiang, and M. Sun, "Effect of in-situ water content variation on the spatial variation of strength of deep cement-mixed clay," *Géotechnique*, vol. 5, no. 69, pp. 351–405, 2019.

[32] F. Favre, P. Boivin, and M. C. S. Wopereis, "Water movement and soil swelling in a dry, cracked vertisol," *Geoderma*, vol. 78, no. 1-2, pp. 113–123, 1997.

[33] T. Sander and H. H. Gerke, "Preferential flow patterns in paddy fields using a dye tracer," *Vadose Zone Journal*, vol. 6, no. 1, pp. 105–115, 2007.

[34] K. Yao, D. An, W. Wang, N. Li, C. Zhang, and A. Zhou, "Effect of nano-mgo on mechanical performance of cement stabilized silty clay," *Marine Georesources and Geotechnology*, vol. 2, no. 20, pp. 250–255, 2020.

[35] C. Li, A. Zhou, and P. Jiang, "Eccentric bearing capacity of embedded strip footings placed on slopes," *Computers and Geotechnics*, vol. 119, Article ID 103352, 2020.
[36] L. Radoslaw and F. Michalowski, "Cracks in slopes: limit analysis approach to stability assessment," *Geocongress*, vol. 1, no. 2012, pp. 442–450, 2012.
[37] R. L. Michalowski, "Stability assessment of slopes with cracks using limit analysis," *Canadian Geotechnical Journal*, vol. 50, no. 10, pp. 1011–1021, 2013.
[38] S. Utili and A. H. Abd, "On the stability of fissured slopes subject to seismic action," *International Journal for Numerical and Analytical Methods in Geomechanics*, vol. 40, no. 5, pp. 785–806, 2016.
[39] K. Krabbenhoft, A. V. Lyamin, M. Hjiaj, and S. W. Sloan, "A new discontinuous upper bound limit analysis formulation," *International Journal for Numerical Methods in Engineering*, vol. 63, no. 7, pp. 1069–1088, 2005.
[40] A. V. Lyamin and S. W. Sloan, "Lower bound limit analysis using non-linear programming," *International Journal for Numerical Methods in Engineering*, vol. 55, no. 5, pp. 573–611, 2002.
[41] H. Ciria, J. Peraire, and J. Bonet, "Mesh adaptive computation of upper and lower bounds in limit analysis," *International Journal for Numerical Methods in Engineering*, vol. 75, no. 8, pp. 899–944, 2008.
[42] J. J. Muñoz, J. Bonet, A. Huerta, and J. Peraire, "Upper and lower bounds in limit analysis: adaptive meshing strategies and discontinuous loading," *International Journal for Numerical Methods in Engineering*, vol. 77, no. 4, pp. 471–501, 2009.
[43] J. Herskovits, P. Mappa, E. Goular, and C. Soares, "Mathematical programming models and algorithms for engineering design optimization," *Computer Methods in Applied Mechanics and Engineering*, vol. 194, no. 30–33, pp. 3244–3268, 2005.
[44] W. Wang, Y. Fu, C. Zhang, N. Li, and A. Zhou, "Mathematical models for stress-strain behavior of nano magnesia-cement-reinforced seashore soft soil," *Mathematics*, vol. 456, p. 8, 2020.
[45] A. Johari and A. M. Lari, "System reliability analysis of rock wedge stability considering correlated failure modes using sequential compounding method," *International Journal of Rock Mechanics and Mining Sciences*, vol. 82, pp. 61–70, 2016.